

Faraday Rotation Measure due to the Intergalactic Magnetic Field

Takuya Akahori¹ and Dongsu Ryu^{2,3}

¹*Research Institute of Basic Science, Chungnam National University, Daejeon, Korea:
akataku@canopus.cnu.ac.kr*

²*Department of Astronomy and Space Science, Chungnam National University, Daejeon,
Korea: ryu@canopus.cnu.ac.kr*

ABSTRACT

Studying the nature and origin of the intergalactic magnetic field (IGMF) is an outstanding problem of cosmology. Measuring Faraday rotation would be a promising method to explore the IGMF in the large-scale structure (LSS) of the universe. We investigated the Faraday rotation measure (RM) due to the IGMF in filaments of galaxies using simulations for cosmological structure formation. We employed a model IGMF based on turbulence dynamo in the LSS of the universe; it has an average strength of $\langle B \rangle \sim 10$ nG and a coherence length of several $\times 100 h^{-1}$ kpc in filaments. With the coherence length smaller than path length, the inducement of RM would be a random walk process, and we found that the resultant RM is dominantly contributed by the density peak along line of sight. The rms of RM through filaments at the present universe was predicted to be ~ 1 rad m^{-2} . In addition, we predicted that the probability distribution function of $|RM|$ through filaments follows the log-normal distribution, and the power spectrum of RM in the local universe peaks at a scale of $\sim 1 h^{-1}$ Mpc. Our prediction of RM could be tested with future instruments.

Subject headings: intergalactic medium — large-scale structure of universe — magnetic fields — polarization

³Author to whom any correspondence should be addressed.

1. Introduction

The intergalactic medium (IGM) contains gas, which was heated mostly by cosmological shocks (Ryu et al. 2003), along with dark matter; the hot gas with $T > 10^7$ K is found inside and around clusters/groups of galaxies and the warm-hot intergalactic medium (WHIM) with $T = 10^5 - 10^7$ K resides mostly in filaments of galaxies, while lower temperature gas is distributed mostly as sheetlike structures or in voids (Cen & Ostriker 1999; Kang et al. 2005). As the gas in the interstellar medium, the gas in the intracluster medium (ICM) and filaments is expected to be permeated with magnetic fields. Measuring Faraday rotation, the rotation of the plane of linearly-polarized light due to the birefringence of magneto-ionic medium, has been one of a few methods to explore the intergalactic magnetic field (IGMF).

Observational exploration of the IGMF using Faraday rotation measure (RM) was started with the investigation of the intracluster magnetic field (ICMF) (see Carilli & Taylor 2002, for a review). An RM study of the Coma cluster, for instance, revealed the ICMF of the strength of order $\sim \mu\text{G}$ for the coherent length of order ~ 10 kpc (Kim et al. 1990). For Abell clusters, the RM of typically $\sim 100 - 200$ rad m^{-2} was observed, indicating an average strength of the ICMF to be $\sim 5-10 \mu\text{G}$ (Clarke et al. 2001; Clarke 2004). RM maps of clusters were analyzed to study the power spectrum of turbulent magnetic fields in the ICM; for instance, a Kolmogorov-like spectrum with a bending at a few kpc scale was found in the cooled core region of the Hydra cluster (Vogt & Enßlin 2005), and spectra consistent with the Kolmogorov spectrum were reported in the wider ICM for the Abell 2382 cluster (Guidetti et al. 2008) and for the Coma cluster (Bonafede et al. 2010).

The nature of the IGMF in filaments, on the contrary, remains largely unknown, because the study of RM outside clusters is still scarce (e.g., Xu et al. 2006); detecting the RM due to the IGMF in filaments is difficult with current facilities, and also removing the galactic foreground is not a trivial task. The next generation radio interferometers including the Square Kilometer Array (SKA), and upcoming SKA pathfinders, the Australian SKA Pathfinder (ASKAP) and the South African Karoo Array Telescope (MeerKAT), as well the Low Frequency Array (LOFAR), however, are expected to be used to study the RM. Particularly, the SKA could measure RM for $\sim 10^8$ polarized extragalactic sources across the sky with an average spacing of ~ 60 arcsec between lines of sight (LOS's) (see, e.g., Carilli & Rawlings 2004; Krause et al. 2009, and references therein), enabling us to investigate the IGMF in the large-scale structure (LSS) of the universe.

Attempts to theoretically predict the RM due to the IGMF have been made: for instance, Ryu et al. (1998) and Dolag et al. (2005) used hydrodynamic simulations for cosmological structure formation to study RM in the LSS, and more recently Dubios & Teyssier (2008) used MHD simulations to study RM for clusters. However, the properties of the

IGMF, especially in filaments, such as the strength and coherence length as well as the spatial distribution, are largely unknown, hindering the theoretical study of RM in the LSS of the universe.

Recently, Ryu et al. (2008) proposed a physically motivated model for the IGMF, in which a part of the gravitational energy released during structure formation is transferred to the magnetic field energy as a result of the turbulent dynamo amplification of weak seed fields in the LSS of the universe. In the model, the IGMF follows largely the matter distribution in the cosmic web and the strength is predicted to be $\langle B \rangle \sim 10$ nG in filaments. Cho & Ryu (2009) studied various characteristic length scales of magnetic fields in turbulence with very weak or zero mean magnetic field, and showed that the coherence length defined for RM is 3/4 times the integral scale in the incompressible limit. They predicted that in filaments, the coherence length for RM would be a few $\times 100 h^{-1}$ kpc with the IGMF of Ryu et al. (2008) and the RM due to the magnetic field would be of order ~ 1 rad m^{-2} .

In this paper, we study RM in the LSS of the universe, focusing on RM through filaments, using simulations for cosmological structure formation along with the model IGMF of Ryu et al. (2008) and Cho & Ryu (2009). Specifically, we present the spatial distribution, probability distribution function (PDF) and power spectrum of the RM, and discuss the prospect of possible observations of the RM. In sections 2 and 3, we describe our model and the results. Discussion is in Section 4, and Summary and Conclusion follows in Section 4.

2. Model

To investigate RM in the LSS of the universe, we used structure formation simulations for a concordance Λ CDM universe with the following values of cosmological parameters: $\Omega_{\text{BM}} = 0.043$, $\Omega_{\text{DM}} = 0.227$, $\Omega_{\Lambda} = 0.73$, $h \equiv H_0/(100 \text{ km s}^{-1} \text{ Mpc}^{-1}) = 0.7$, $n = 1$, and $\sigma_8 = 0.8$ (same as in Ryu et al. 2008). They were performed using a particle-mesh/Eulerian, cosmological hydrodynamic code (Ryu et al. 1993). A cubic region of comoving volume $(100 h^{-1} \text{ Mpc})^3$ was reproduced with 512^3 uniform grid zones for gas and gravity and 256^3 particles for dark matter, so the spatial resolution is $195 h^{-1}$ kpc. Sixteen simulations with different realizations of initial condition were used to compensate cosmic variance.

For the IGMF, we employed the model of Ryu et al. (2008); it proposes that turbulent-flow motions are induced via the cascade of the vorticity generated at cosmological shocks during the formation of the LSS of the universe, and the IGMF is produced as a consequence of the amplification of weak seed fields of any origin by the turbulence. Then, the energy density (or the strength) of the IGMF can be estimated with the eddy turnover number and

the turbulent energy density as follow:

$$\varepsilon_B = \phi \left(\frac{t}{t_{\text{eddy}}} \right) \varepsilon_{\text{turb}}. \quad (1)$$

Here, the eddy turnover time is defined as the reciprocal of the vorticity at driving scales, $t_{\text{eddy}} \equiv 1/\omega_{\text{driving}}$ ($\vec{\omega} \equiv \vec{\nabla} \times \vec{v}$), and ϕ is the conversion factor from turbulent to magnetic energy that depends on the eddy turnover number t/t_{eddy} . The eddy turnover number was estimated as the age of universe times the magnitude of the local vorticity, that is, $t_{\text{age}} \omega$. The local vorticity and turbulent energy density were calculated from simulations for cosmological structure formation described above. A functional form for the conversion factor was derived from a separate, incompressible, magnetohydrodynamic (MHD) simulation of turbulence dynamo. For the direction of the IGMF, we used that of the passive fields from simulations for cosmological structure formation, in which weak seed fields were evolved passively, ignoring the back-reaction, along with flow motions (Kulsrud et al. 1997; Ryu et al. 1998).

In our model, as seed magnetic fields, we took the ones generated through the Biermann battery mechanism (Biermann 1950) at cosmological shocks. There are, on the other hand, a number of mechanisms that have been suggested to create seed fields in the early universe. Besides various inflationary and string theory mechanisms, the followings include a partial list of astrophysical mechanisms. At cosmological shocks, in addition, Weibel instability can operate and produce magnetic fields (Medvedev et al. 2006; Schlickeiser & Shukla 2003), and streaming cosmic rays accelerated by the shocks can amplify weak upstream magnetic fields via non-resonant growing mode (Bell 2004). In addition, for instance, galactic outflows during the starburst phase of galactic evolution (Donnert et al. 2009) and the return current induced by cosmic-rays produced by Supernovae of first stars (Miniati & Bell 2010) were suggested to deposit seed fields. We point, however, that in our model the IGMF resulting from turbulent amplification should be insensitive to the origin of seed fields.

The spatial distribution of the strength of the resulting IGMF is shown in Figure 4 of Ryu et al. (2008) and Figure 1 of Ryu et al. (2010). It is very well correlated with the distribution of matter. The average strength of our model IGMF for the WHIM with $10^5 < T < 10^7$ K in filaments is $\langle B \rangle \sim 10$ nG, $\langle B^2 \rangle^{1/2} \sim \text{a few} \times 10$ nG, $\langle \rho B \rangle / \langle \rho \rangle \sim 0.1$ μ G, or $\langle (\rho B)^2 \rangle^{1/2} / \langle \rho^2 \rangle^{1/2} \sim \text{a few} \times 0.1$ μ G.

3. Results

We calculated RM, defined as $\Delta\chi/\Delta\lambda^2$ (χ is the rotation angle of linearly-polarized light at wavelength λ), in the local universe with $z = 0$ along a path length of $L = 100 h^{-1}$

Mpc, which is the box size of structure formation simulations. Figure 1 shows the resulting RM map of $(28 h^{-1}\text{Mpc})^2$ area in logarithmic and linear scales. RM traces the large-scale distribution of matter, and we see two clusters and a filamentary structure containing several groups. Through the clusters, groups, and filament in the field, RM is roughly ~ 100 , ~ 10 , and ~ 1 , respectively, while RM through sheets and voids is much less. The bottom panel of Figure 1 shows the mixture of positive and negative RM, reflecting the randomness of magnetic fields in the LSS.

With the coherence length of magnetic fields for RM (see Discussion) expected to be smaller than the path length which should be a cosmological scale, the inducement of RM is expected to be a random walk process. Figure 2 shows the distributions of RM as well as other quantities along a few LOS's through filaments; it confirms that the inducement of RM is indeed a random walk process. However, we note that the resulting RM is dominated by the contribution from the density peak along LOS's.

To quantify RM in the LSS of the universe, we calculated the probability distribution function (PDF) of $|\text{RM}|$ for $512^2 \times 3 \times 16$ (projected grid zones \times directions \times runs) LOS's. Figure 3 shows the resulting PDF through the LOS's of different ranges of the mean temperature weighted with X-ray emissivity, T_X . The figure also shows the fitting to the log-normal distribution,

$$\text{PDF}(\log_{10} |\text{RM}|) = \frac{1}{\sqrt{2\pi\sigma^2}} \exp \left[-\frac{(\log_{10} |\text{RM}| - \mu)^2}{2\sigma^2} \right], \quad (2)$$

finding that the PDF closely follows the log-normal distribution. We also calculated the root mean square (rms) of RM, $\langle \text{RM} \rangle_{\text{rms}}$; note that the mean of RM, $\langle \text{RM} \rangle$, is zero for our IGMF. Through the WHIM, which mostly composes filaments, $\langle \text{RM} \rangle_{\text{rms}} = 1.41 \text{ rad m}^{-2}$. This agrees well with the value predicted with the mean strength and coherence length of the IGMF in filaments by Cho & Ryu (2009). However, this is an order of magnitude smaller than the values of $|\text{RM}|$ toward the Hercules and Perseus-Pisces superclusters reported in Xu et al. (2006). The difference is mostly due to the mass-weighted path length; the value quoted by Xu et al. (2006) is about two orders of magnitude larger than ours. Through the hot gas with $10^7 < T < 10^8 \text{ K}$, $\langle \text{RM} \rangle_{\text{rms}} = 108 \text{ rad m}^{-2}$, which is in good agreement with RM observations of galaxy clusters (Clarke et al. 2001; Clarke 2004). Through the hot gas, however, we found RM of up to $\gtrsim 1000 \text{ rad m}^{-2}$. This should be an artifact of limited resolution (see Discussion). So the values for the hot gas in our work should not be taken seriously.

Finally, we calculated the two-dimensional power spectrum of RM on 3×16 (directions \times runs) projected planes; $P_{\text{RM}}(k) \sim |\text{RM}(\vec{k})|^2 k$, where $\text{RM}(\vec{k})$ is the Fourier transform of $\text{RM}(\vec{x})$ on planes. Figure 4 shows the resulting power spectrum along with the power spectra of electron density, magnetic fields, and the curl component of flow motions, \vec{v}_{curl} , which

satisfies the relation $\vec{\nabla} \times \vec{v}_{\text{curl}} \equiv \vec{\nabla} \times \vec{v}$. The power spectrum of RM peaks at $k \sim 100$, which corresponds to $\sim 1 h^{-1}$ Mpc. Cosmic variance is not significant around the peak, although it is larger at smaller k , as expected. The power spectrum of RM reflects the spatial distributions of electron density, n_e , and LOS magnetic field, B_{\parallel} . The power spectra of projected n_e and projected B_{\parallel} , have peaks at $\sim 3 h^{-1}$ Mpc and $\sim 1.5 h^{-1}$ Mpc, respectively. The shape of the power spectrum of RM follows that of projected B_{\parallel} rather than that of projected n_e , implying that the statistics of RM would primarily carry the statistics of the IGMF.

4. Discussion

Our results depend of RM on the strength and coherence length of the IGMF. We employed a model where the strength of the local IGMF was estimated based on turbulence dynamo, while the direction was gripped from structure formation simulations with passive fields (see Section 2). In principle, if we had performed full MHD simulations, we could have followed the amplification of the IGMF through turbulence dynamo along with its direction. In practice, however, the currently available computational resources do not allow a numerical resolution high enough to reproduce the full development of MHD turbulence. Since the numerical resistivity is larger than the physical resistivity by many orders of magnitude, the growth of magnetic fields is expected to be saturated before dynamo action becomes fully operative (see, e.g., Kulsrud et al. 1997). In such situation, the state of magnetic fields in full MHD, including, for instance, the power spectrum, is expected to mimic that of passive fields. This is the reason why we adopted the model of Ryu et al. (2008) to estimate the strength of the IGMF, but we still used passive fields from structure formation simulations to model the field direction.

The validity of our model IGMF was checked as follows:

- 1) In MHD turbulence, the distribution of magnetic fields, including the direction, is expected to correlate with that of vorticity, since magnetic fields and vorticity are described by similar equations except the baroclinity term in the equation for vorticity (if dissipative processes are ignored) (see, e.g., Kulsrud et al. 1997). Such a correlation can be clearly seen in Figure 5, in which we depicts the distributions of our IGMF and vorticity in two-dimensional slices.
- 2) Full MHD turbulence simulations suggest that the peak of magnetic field spectrum occurs $\sim 1/2$ of the energy injection scale, or the peak scale of velocity power spectrum, at saturation; in the linear growth stage, the peak scale of magnetic field spectrum grows as $\sim t^{1.5}$ or so (Cho & Ryu 2009). With our model IGMF, the peak scale of magnetic field spectrum

is $\sim 1 h^{-1}$ Mpc (the third panel of Figure 4); on the other hand, the curl component of flow motions has the peak of power spectrum at $\sim 4 h^{-1}$ Mpc (the bottom panel of Figure 4). That is, the peak scale of magnetic field spectrum is $\sim 1/4$ of the energy injection scale in our model IGMF. By considering the turbulence in the LSS of the universe has not yet reached the fully saturated stage (see, e.g., Ryu et al. 2008), the ratio of the two scales seems to be feasible.

These suggest that our model IGMF would produce reasonable results, although eventually it needs to be replaced with that from full MHD simulations for cosmological structure formation when computational resources allow such simulations in future.

Apart from our model for the IGMF, the finite numerical resolution of simulations could affect our results. The average strength of our model IGMF is $\langle B \rangle \sim$ a few μG in clusters/groups, $\sim 0.1\mu\text{G}$ around clusters/groups, and ~ 10 nG in filaments. Ryu et al. (2008) tested the numerical convergence of the estimation. With simulations of different numerical resolutions for cosmological structure formation, it was shown that $\langle B \rangle$ of our model IGMF for the WHIM with $10^5 < T < 10^7$ K would approach the convergence value within a factor $\sim 2 - 3$ at the resolution of 512^3 grids (see Figure S5 of SOM of Ryu et al. (2008)).

It is, on the other hand, rather tricky to assess the effect of finite resolution on the coherence length of our model IGMF, because the definition of coherence length for RM is not completely clear and the estimation of coherence length, for instance, for the filament IGMF alone is not trivial. We tried to quantify coherence length in the following three ways: 1) We directly calculated the coherence length of B_{\parallel} , that is, the length with the same sign of B_{\parallel} , along LOS's. Figure 6 shows the PDF of the resulting coherence length through the WHIM, which composes mostly filaments. It peaks at the length of 3 zones corresponding to $586 h^{-1}$ kpc. 2) We calculated $3/4$ times the integral scale,

$$\frac{3}{4} \times 2\pi \frac{\int P_B^{3D}(k)/k dk}{\int P_B^{3D}(k) dk}, \quad (3)$$

which is the coherence length defined for RM in the incompressible limit (see Introduction), for the IGMF inside the whole computational box of $(100 h^{-1}\text{Mpc})^3$ volume. Here, $P_B^{3D}(k)$ is the three-dimensional power spectrum of magnetic fields (the third panel of Figure 4). We found the value to be $\sim 800 h^{-1}$ kpc for our model IGMF. 3) We also calculated the largest energy containing scale in the whole computational box, which is the peak scale of $kP_B^{3D}(k)$ (not shown). It is $\sim 900 h^{-1}$ kpc for our model IGMF. Note that the latter two values include contributions from the IGMF in filaments as well as in clusters, sheets, and voids. All the three scales are comparable. These length scales are ~ 3 to 5 times larger than the grid resolution of our simulations, $195 h^{-1}$ kpc.

Cho & Ryu (2009) studied characteristic lengths in incompressible simulations of MHD turbulence (see Introduction); based on it, they predicted that the coherence length for RM would be a few $\times 100 h^{-1}$ kpc in filaments, while a few $\times 10 h^{-1}$ kpc in clusters. With our grid resolution of $195 h^{-1}$ kpc, the coherence length of the IGMF in clusters should not be resolved and so our estimation of RM for clusters should be resolution-affected, as pointed in Section 3. On the other hand, while the predicted coherence length for the IGMF in filaments is still larger than the grid resolution, the estimated coherence length of B_{\parallel} for the WHIM is a couple of times larger than the prediction for filaments. It could be partly due to the limited resolution in our simulations. However, as noted in Section 3, RM is dominantly contributed by the density peak along LOS's (Figure 2).

The above statements indicate that our estimate of the RM through filaments is expected to have uncertainties, especially due to limited resolution of our simulations; the error in our estimation could be up to a factor of several.

5. Summary and Conclusion

We studied RM in the LSS of the universe, focusing on RM through filaments; simulations for cosmological structure formation were used and the model IGMF of Ryu et al. (2008) and Cho & Ryu (2009) based on turbulence dynamo was employed. Our findings are summarized as follows. 1) With our model IGMF, the rms of RM through filaments at the present universe is $\sim 1 \text{ rad m}^{-2}$. 2) The PDF of $|\text{RM}|$ through filaments follows the log-normal distribution. 3) The power spectrum of RM due to the IGMF in the local universe peaks at a scale of $\sim 1 h^{-1}$ Mpc. 4) Within the frame of our model IGMF, we expect that the uncertainty in our estimation for the rms of RM through filaments, due to the finite numerical resolution of simulations, would be a factor of a few.

We note that our model does not include other possible contributions to the IGMF, for instance, that from galactic black holes (AGN feedbacks) (see, e.g., Kronberg et al. 2001). So our model may be regarded as a minimal model, providing a baseline for the IGMF. With such contributions, the real IGMF might be somewhat stronger, resulting in somewhat larger RM.

It has been suggested that future radio observatories such as LOFAR, ASKAP, MeerKAT and SKA could detect the extragalactic RM of $\sim 1 \text{ rad m}^{-2}$ we predict (see, e.g., Beck 2009). However, it is known that the typical galactic foreground of RM is a few tens and of order ten rad m^{-2} in the low and high galactic latitudes, respectively (see, e.g., Simard-Normandin & Kronberg 1980). So the detection of the extragalactic RM of \sim

1 rad m⁻² or so could be possible only after the galactic foreground is removed. We note, however, that with filaments at cosmological distance, the peak of the power spectrum of the RM due to the IGMF in filaments would occur at small angular scales; for instance, for a filament at a distance of 100 h^{-1} Mpc, the peak would occur at ~ 0.5 degree or so. This is much smaller than the expected angular scale of the peak of the galactic foreground, which would be around tens degree (see, e.g., Frick et al. 2001). Then, it would be plausible to extract the signature of the RM of ~ 1 rad m⁻² due to the IGMF in filaments. We leave this issue and connecting our theoretical prediction of RM in the LSS of the universe to observation for future studies.

TA was supported in part by National Research Foundation of Korea (R01-2007-000-20196-0). DR was supported in part by National Research Foundation of Korea (K20901001400-09B1300-03210)

REFERENCES

- Bell, A. R. 2004, MNRAS, 353, 550
- Biermann, L. 1950, Z. Naturforsch, A, 5, 65
- Beck, R. 2009, Rev. Mexicana Astron. Astrofis.(Serie de Conferencias), 36, 1
- Bonafede, A., Feretti, L., Murgia, M., Govoni, F., Giovannini, G., Dallacasa, D., Dolag, K., & Taylor, G. B. 2010, to appear in A&A(arXiv:1002.0594)
- Carilli, C. L. & Taylor, G. B. 2002, ARA&A, 40, 319
- Carilli, C. L. & Rawlings S. 2004, New A Rev., 48, 1
- Cen, R. & Ostriker, J. P. 1999, ApJ, 514, 1
- Cho, J., Vishniac, E. T., Beresnyak, A., Lazarian, A., & Ryu, D. 2009, ApJ, 693, 1449
- Cho, J., & Ryu, D. 2009, ApJ, 705, L90
- Clarke, T. E., Kronberg, P. P., & Böhlinger, H. 2001, ApJ, 547, L111
- Clarke, T. E. 2004, J. Korean Astron. Soc. 37, 337
- Donnert, J., Dolag, K., Lesch, H., & Müller, E. 2009, MNRAS, 392, 1008

- Dolag, K., Crasso, D., Springel, V., & Tkachev, I. 2005, *J. Cosmology Astropart. Phys.*, 1, 9
- Dubios, Y. & Teyssier, R. 2008, *A&A*, 482, L13
- Frick, P., Stepanov, R., Shikurov, A., & Sokoloff, D. 2001, *MNRAS*, 325, 649
- Guidetti, D., Murgia, M., Govoni, F., Parma, P., Gregorini, L., deRuiter, H. R., Cameron, R. A., & Fanti, R. 2008, *A&A*, 483, 699
- Kang, H., Ryu, D., Cen, R., & Song, D. 2005, *ApJ*, 620, 21
- Kim, K. T., Kronberg, P. P., Dewdney, P. D., & Landecker, T. L. 1990, *ApJ*, 355, 29
- Krause, M., Alexander, P., Bolton, R., Geisbüsch, J., Green, D. A., & Riley, J. 2009, *MNRAS*, 400, 646
- Kronberg, P. P., Dufton, Q. W., Li, H., & Colgate, S. A. 2001, *ApJ*, 560, 178
- Kulsrud, R. M., Cen, R., Ostriker, J. P., & Ryu, D. 1997, *ApJ*, 480, 481
- Medvedev, M. V., Silva, L. O., & Kamionkowski, M. 2006, *ApJ*, 642, L1
- Miniati, F. & Bell, A. R. 2010, arXiv:1001.2011
- Ryu, D., Das, S., & Kang, H. 2010, *ApJ*, 710, 1422
- Ryu, D., Kang, H., & Biermann, P. L. 1998, *A&A*, 335, 19
- Ryu, D., Kang, H., Cho, J., & Das, S. 2008, *Science*, 320, 909
- Ryu, D., Kang, H., Hallman, E., & Jones, T. W. 2003, *ApJ*, 593, 599
- Ryu, D., Ostriker, J. P., Kang, H., & Cen, R. 1993, *ApJ*, 414, 1
- Schlickeiser, R., & Shukla, P. K. 2003, *ApJ*, 599, L57
- Simard-Normandin, M. & Kronberg, P. P. 1980, *ApJ*, 242, 74
- Xu, Y., Kronberg, P. P., Habib, S., & Dufton, Q. W. 2006, *ApJ*, 637, 19
- Vogt, C. & Enßlin, T. A. 2005, *A&A*, 434, 67

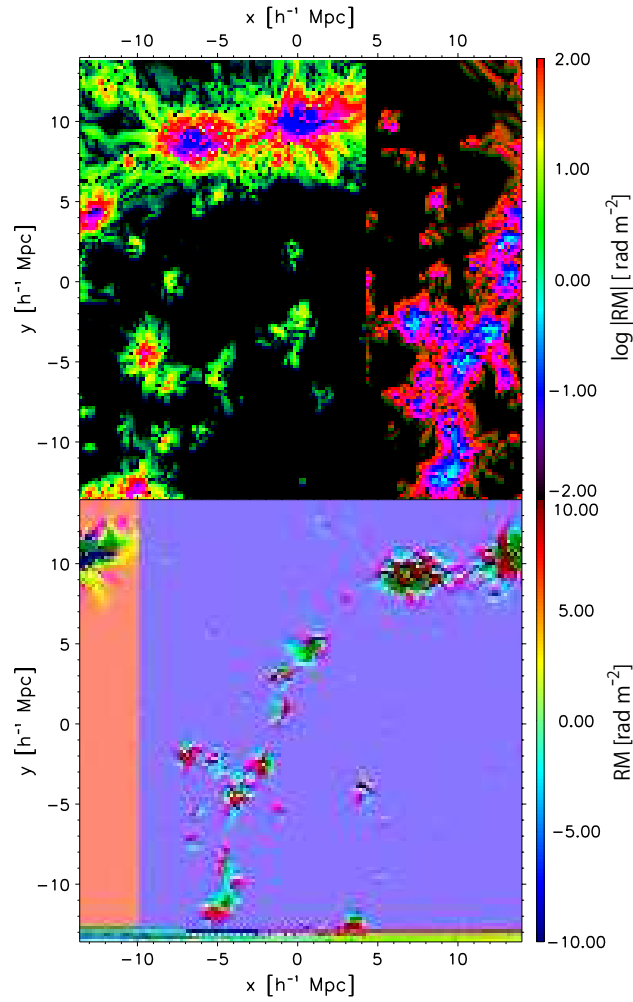


Fig. 1.— RM map of $(28 h^{-1} \text{Mpc})^2$ area in the local universe of depth (path length) of $L = 100 h^{-1}$. Top and bottom panels show the map in logarithmic and linear scales, respectively.

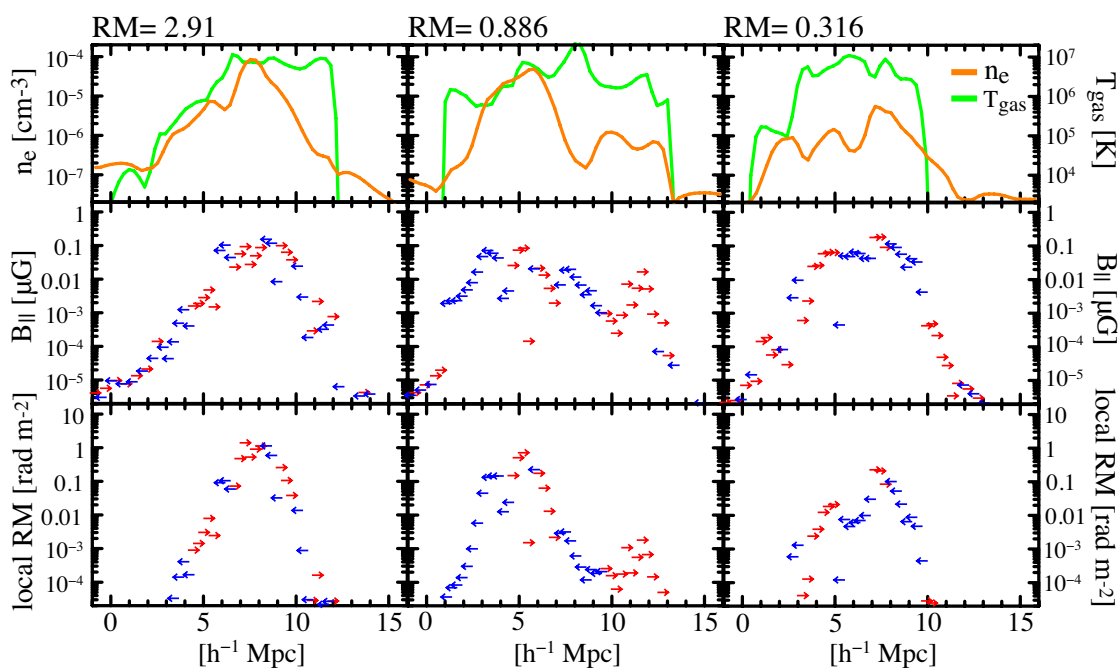


Fig. 2.— Profiles of local RM, LOS magnetic field, B_{\parallel} , electron density, n_e , and gas temperature, T , along a few LOS's through filaments. The arrows indicate the sign of local RM and B_{\parallel} .

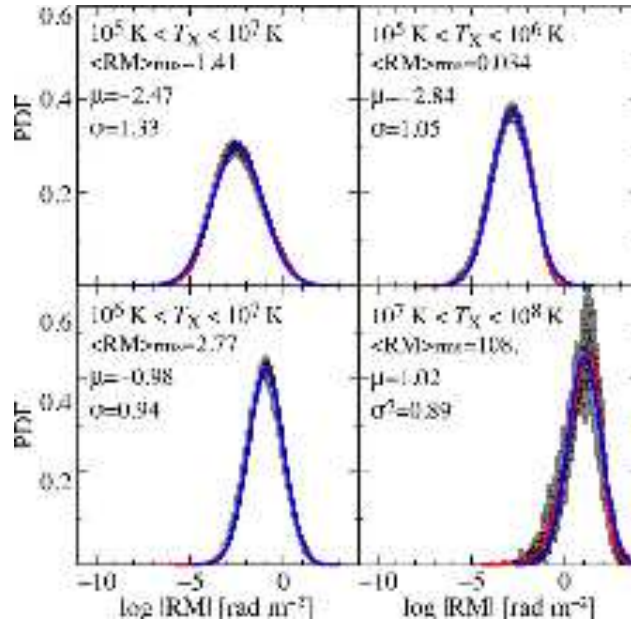


Fig. 3.— PDF of $|\text{RM}|$ through LOS's of different ranges of the mean temperature weighted with X-ray emissivity, T_X . Thin lines, thick lines (red or black), and thick lines (blue or gray) show the PDFs from 16 independent runs, their average, and the best-fit to the log-normal distribution, respectively. The values of fitting parameters and the rms of RM are also shown.

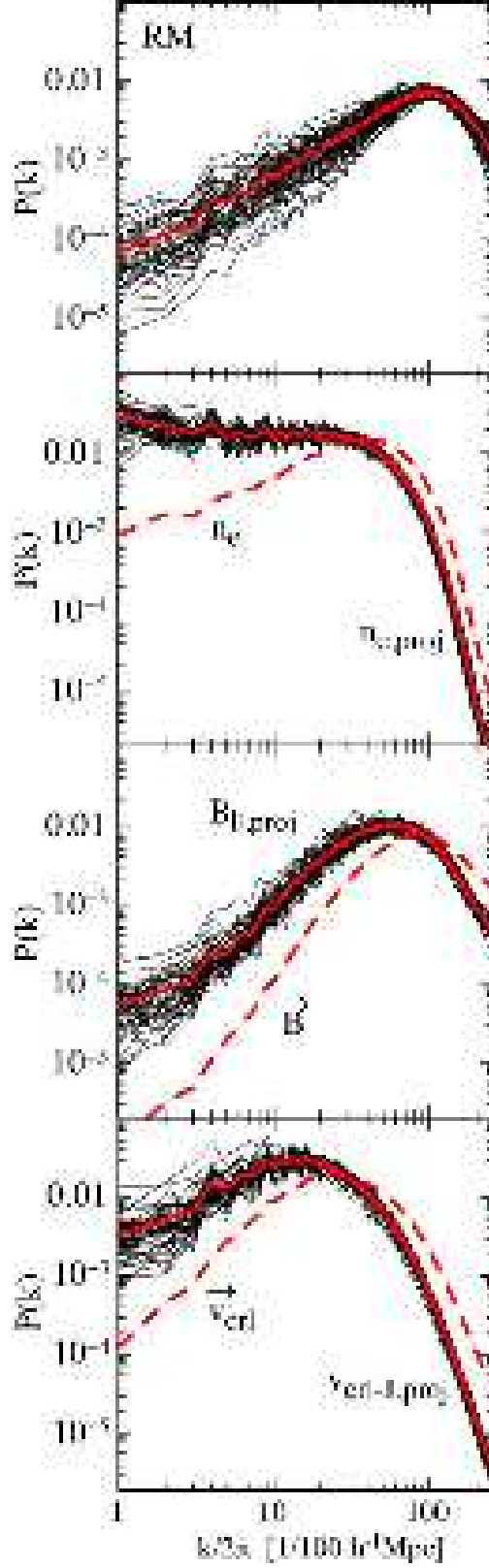


Fig. 4.— Two-dimensional power spectra of RM, projected electron density ($n_{e,\text{proj}}$), projected line-of-sight IGMF strength ($B_{\parallel,\text{proj}}$), and projected curl component of flow motions (\vec{v}_{curl}) from top to bottom panels, respectively. Thin solid lines show the power spectra for 3×16 two-dimensional maps, and thick solid lines show their average. The three-dimensional power spectra of n_e , \vec{B} , and \vec{v}_{curl} , are also shown with thick dashed lines.

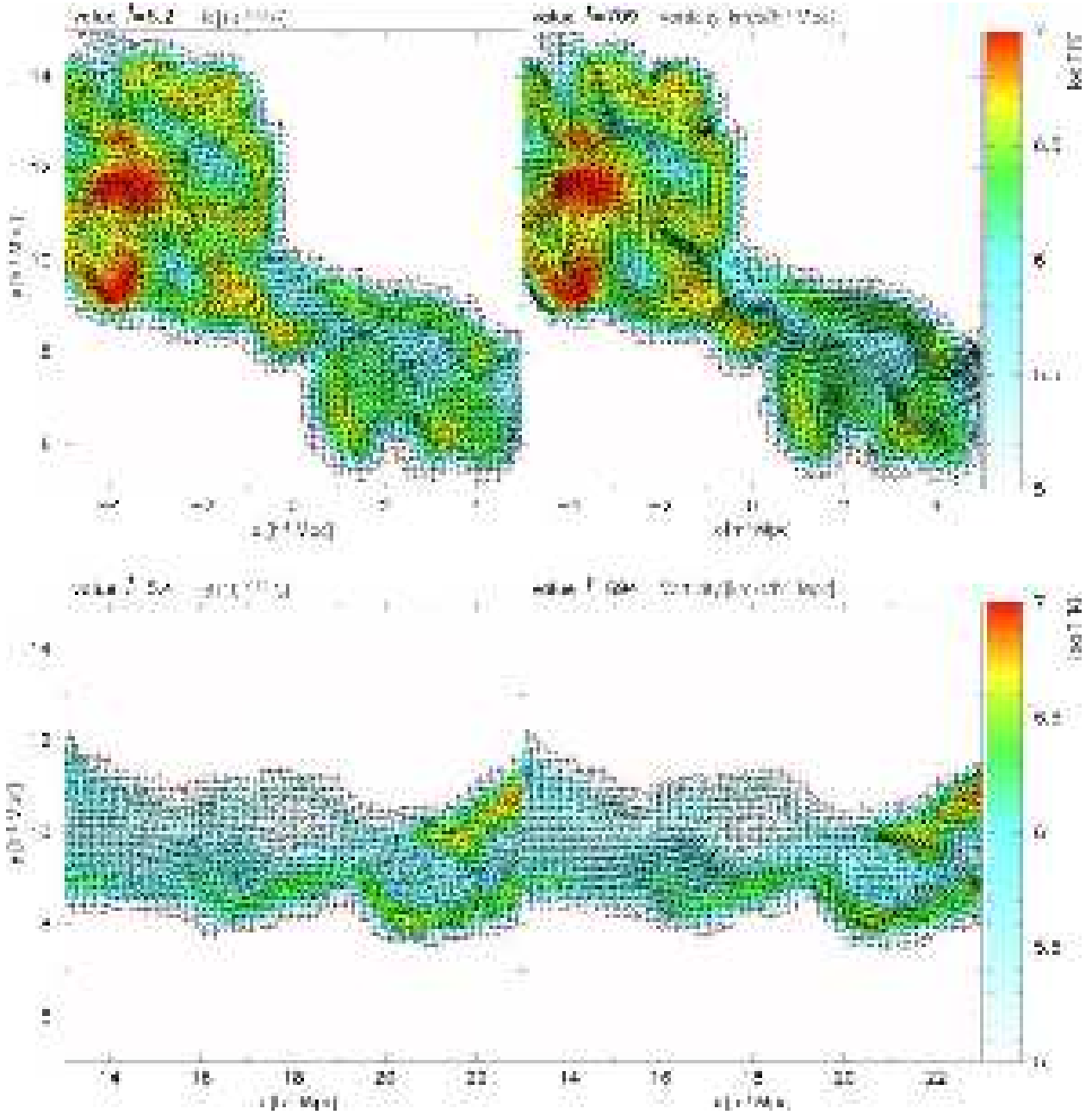


Fig. 5.— Distributions of the IGMF (left) and vorticity (right) in two-dimensional slices. The length of arrows for the IGMF corresponds to x of 10^{x-12} G. The color shows the gas temperature.

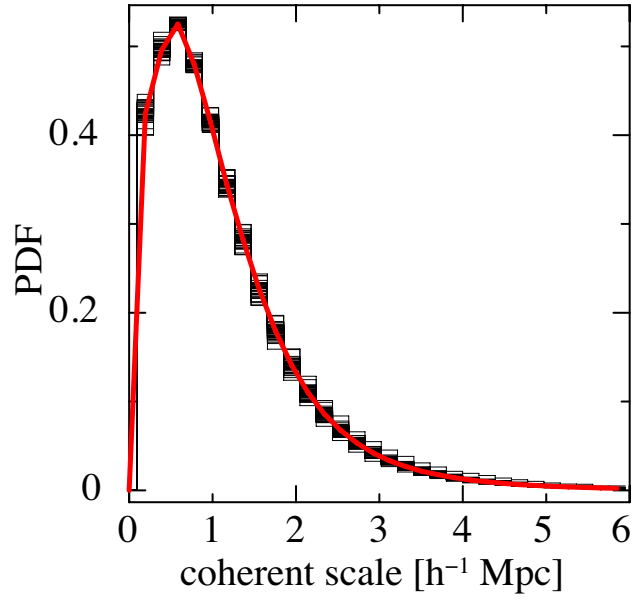


Fig. 6.— PDF of the coherence length of B_{\parallel} along LOS's (the length with the same sign of B_{\parallel}) through the WHIM. Thin and thick lines show the PDFs for 16 independent runs and their average, respectively.